Chemical Engineering Science 158 (2017) 21–29

Contents lists available at ScienceDirect

Chemical Engineering Science

journal homepage: www.elsevier.com/locate/ces

Numerical simulation of separation process for enhancing fine particle removal in tertiary sedimentation tank mounting adjustable baffle

Hong Guo [a], Seo Jin Ki [a], Seungjae Oh [b], Young Mo Kim [a], Semyung Wang [b], Joon Ha Kim [a,*]

[a] School of Environmental Science and Engineering, Gwangju Institute of Science and Technology (GIST), Gwangju 500-712, Republic of Korea
[b] School of Mechatronics, GIST, Gwangju 500-712, Republic of Korea

HIGHLIGHTS

- The hydraulic behavior of a sedimentation tank was studied using the finite element method.
- The sedimentation tank was equipped with adjustable baffles to better analyze particle settling.
- The simulation results matched well with the experimental data.
- The particle removal efficiency varied considerably by varying the angles of the adjustable baffle.
- The results can be used to design a compact sedimentation tank for aquaculture farming.

ARTICLE INFO

Article history:
Received 3 June 2016
Received in revised form
18 August 2016
Accepted 16 September 2016
Available online 19 September 2016

Keywords:
Separation process
Finite element method
Fine particle removal
Adjustable baffle
Sedimentation tank
Hydraulic behavior

ABSTRACT

The presence of flow control devices and/or obstacles in the fluid flow such as baffles and spacers complicates the solid-fluid mixing pattern, which remains difficult to describe by classical analytical solutions. In this study, the removal of fine particles in a tertiary sedimentation tank mounting an adjustable baffle was investigated using the computational fluid dynamics code-COMSOL. The solid-fluid motion was solved by consecutively applying the equations of the continuity and momentum using the finite element method. The experiment was conducted by the sedimentation tank with the adjustable baffle inclined at 30° in a pilot scale plant. It's used as the reference data set for numerical simulations that were run on a 2-dimensional domain by modifying the configuration settings of angles for an adjustable baffle (i.e., 30°, 45°, and 60°) and without one. Results showed that the simulation results matched well with the experimental data for an adjustable baffle at 30° (NSE=0.97). The sedimentation tank with the adjustable baffle at different angles had a lower overflow rate (in the area of flow rebound) and mixing intensity (in the area of flow curve) than without one, eventually leading to enhanced particle removal efficiency. This tendency became more pronounced as the particle motion stabilized over time. The sedimentation tank mounting the adjustable baffle at 30° provided the best settling efficiency among the four different flow patterns. However, the conventional index that represents the mixing properties did not correctly address their relative efficiency for fine particle removal. Therefore, a numerical simulation tailored to a given geometry should be conducted to fully elucidate the fluid dynamics in the sedimentation tank with complex devices or obstacles.

© 2016 Elsevier Ltd. All rights reserved.

1. Introduction

Fluid dynamics in water treatment systems plays an important role in facilitating the particle removal process and ensuring effective system design in affordable budget (Brouckaert and Buckley, 1999). A sedimentation tank, a popular unit in advanced water treatment processes, is traditionally used to remove suspended solids from turbid water by settling via gravity. The performance of the sedimentation tank is affected by two universal factors, flow patterns and particle properties (Goula et al., 2008b). More precisely, the flow motion is determined by the flow rate or velocity (that determines the turbulence), temperature, and mixing characteristics. The intrinsic particle properties include their size, density, shape, and charge, which affect the ways they interact with water through drag and buoyancy forces. In addition, the geometry of the sedimentation tank is tightly bound to these two dominant factors, which further complicates the description of the hydraulic behavior in the sedimentation tank, specifically in the

* Corresponding author.
E-mail address: joonkim@gist.ac.kr (J.H. Kim).

http://dx.doi.org/10.1016/j.ces.2016.09.022
0009-2509/© 2016 Elsevier Ltd. All rights reserved.

Nomenclature

c_d	particle drag coefficient (dimensionless)
d	diameter (m)
F	volume force (N/m^3)
g	gravity vector (m/s^2)
m	mass (kg)
n	normal vector
p	pressure (Pa)
u'	turbulent fluctuation (m/s)
u	velocity vector (m/s)
U	mean velocity of fluid flow (m/s)
u_{slip}	relative velocity vector between two phases (m/s)
ζ	random number normally distributed with zero mean and unit standard deviation
μ	viscosity (Pa s)
ρ	density (kg/m^3)
τ_{Gm}	sum of viscous and turbulent stresses (kg/m s^2)
τ_p	particle velocity response time (s)
ϕ	volume fraction (dimensionless)
D_{md}	turbulent dispersion coefficient (m^2/s)
m_{dc}	mass transfer rate from dispersed to the continuous phase (kg/(m^3 s)
Re_p	particle Reynolds number (dimensionless)
k	turbulent kinetic energy (m^2/s^3)
ε	dissipation rate of kinetic energy (m^2/s^3)
P_k	production term of turbulence (dimensionless)
F	additional volume force (N/m^3)

Subscripts

c	continuous phase
d	dispersed phase
f	fluid (of water)
p	particle

presence of fluid obstacles or assisted devices (Patziger et al., 2012). Therefore, a physically-based model that can accurately explain these factors is required to effectively design the sedimentation tank in compact size while enhancing the settling of suspended solids.

A mathematical modeling study expedites the design of the sedimentation tank by avoiding trial and error experiments in the lab or via a pilot system. Larsen (1977) developed the original mathematical model for simulating the movement of water only in a rectangular settling tank, and investigated 2-dimensional velocity profiles (i.e., without particles) in a fluid field. Lyn et al. (1992) expanded this original model by including a gravity-density term in particle transport and accounted for the settling of particles of different sizes with respect to the flow velocity. The expanded model, however, did not address the interactions between the liquid and solid phases occurred in a solid-fluid field. Subsequently, Manninen et al. (1996) improved the expanded model using a single governing equation that combined the continuous (for fluids) and dispersed phases (for particles) as two interpenetrating continua, simultaneously solving the continuity and momentum equations of the mixture. This model has since been widely used as a parent for studying the motion of particles or gas bubbles in fluid fields such as membrane bioreactors, gas dispersion reactors, and settling tanks.

Such mathematical models are, however, difficult to analytically solve as geometric complexity of the system (that affects the hydraulic behaviors) is increased progressively. DeVantier and Larock (1986, 1987) applied the finite element method (FEM) to the sedimentation tank to simulate a 2-dimensional turbulent flow in terms of density effects, obtaining a fairly good prediction accuracy while consuming large memory resources. On the other hand, reasonable prediction accuracy was achieved in secondary clarifiers using the finite volume method (FVM), which used less memory than the FEM during the simulation (Szalai et al.,1994). Also McCorquodale et al. (1991), combined the FEM and finite different method (FDM) to examine the effects of particle size on the flow motion in primary clarifiers, but did not find any remarkable advantage over the FEM alone. Out of these methods, the FVM has been preferred in the area of fluid dynamics due to less memory requirements and acceptable accuracy. Combining the FVM with the Euler-Lagrange approach has recently enabled researchers to successfully describe the hydraulic behaviors of flow and particles in the sedimentation tank under the influence of turbulent flow, sludge return, and water temperature (Al-Sammarraee et al., 2009; Goula et al., 2008a; Karama et al., 1999; McCorquodale et al., 1991).

In fact, the transport of the particles, including their interaction with the surrounding fluid, can be numerically elucidated using either the Euler-Euler or Euler-Lagrange approaches (Goula et al., 2008a; Manninen et al., 1996; Tarpagkou and Pantokratoras, 2013; Wang et al., 2013). Two methods were similar in that the fluid was considered as a continuum, but were dissimilar in the particle phase simulation. For instance, the Euler-Euler approach assumed the particles as a piece of a continuous medium (i.e., one of volume fractions), whereas the particle phase was treated separately from the fluid phase (as the Lagrangian discrete field) in the Euler-Lagrange approach (Adamczyk et al., 2014). In a practical aspect, the Euler-Euler method was more easily applied to multiphase flow systems at the field scale than the Euler-Lagrange method due to convenience in experimental methods measuring the parameters (required in the simulation) such as the particle density and diameter. Another advantage of the Euler-Euler approach was that with low computational demand, the particle size, volume fraction, and relative velocity distribution were estimated directly at the end of the simulation. In contrast, the Euler-Lagrange approach provided accurate information on individual particles such as the particle pathway and particle dispersion patterns, allowing the simulation of agglomeration or deformation of the particles in the fluid systems (Zhu et al., 2015). One notable disadvantage was, however, that it required large computational resources for the particles at high concentration, and thus, was rarely used for the simulation of the dense fluidized beds. Also, the absence of a module regarding the collision between the particles, which was normally adopted in the Euler-Euler approach, was another minor drawback in the Euler-Lagrange approach (Loha et al., 2014).

As compared to previous studies, this study explores the effect of geometric complexity on the settling of fine particles in the compact sedimentation unit using the FEM with the Euler-Euler approach This is because the FEM, which can be now implemented affordably due to advances in computational resources, provides a higher prediction accuracy than the FVM for the system with complex geometry (Gohil et al., 2011). For this study, a pilot scale experiment in the sedimentation tank equipped with an adjustable baffle installed at an inlet channel of influent was conducted to investigate the dynamic flow patterns and particle motion, which were then used as a basis for numerical analysis. Using the computation fluid dynamics package COMSOL, this study specifically aims: 1) to identify how the adjustable baffle

inclined at different degrees influences the flow patterns inside the sedimentation tank, as compared to having no baffle; 2) to explain how the motion of particles interacts with the flow patterns in such tank under different configuration settings of angles; and 3) to demonstrate how the traditional index representing the mixing characteristics of a given system helps determine the best angle of the adjustable baffle that enhances efficiency of the fine particle removal.

2. Materials and methods

2.1. Sedimentation tank modeling

The sedimentation tank system used for modeling the hydraulic behaviors with and without the adjustable baffle is illustrated in Fig. 1a and b. The pilot system which was installed at the Environmental Installations Corporation of the Gwangju in Korea had a daily water treatment capacity of 1000 m^3. In the system, two sedimentation tanks were interconnected across the flocculation tank that enhanced the bonding among particulates using flocking agents (Fig. 1a). The system received water that was originally directed into a tertiary water treatment process, passing from the inlet channel after the flocculation tank through the sedimentation tanks (on both sides) to the outlet channel (see thick arrow in Fig. 1a). Note that the height of the inlet is designed to be higher than the outlet of the sedimentation tanks to prevent an overflow..

Inclined plates in the outlet channel were used to equally distribute the flow as well as to stabilize flow patterns, which resulted in enhanced particle sedimentation (Tarpagkou and Pantokratoras, 2014). In the inlet channel, a series of fixed baffles played a role in reducing the flow rate of incoming water, whereas the adjustable baffle installed at the end of the channel provided various types of flow and particle patterns inside the sedimentation tank. For this study, we examined the effect of four different hydraulic behaviors on the removal efficiency of fine particles in the sedimentation tank, by modifying the configuration settings of angles for the adjustable baffle (i.e., 30°, 45°, and 60°) and without one. The pilot system was operated using the adjustable baffle inclined at 30°, which was then compared to the simulation results obtained from the same model configuration. Fig. 1b shows more detailed information of the model domain for left-hand symmetry. Exactly the same geometry, including inclined plates as well as both fixed and adjustable baffles, was created in a computer-aided design (CAD) environment and then imported into the COMSOL using the CAD import module. Identical operating conditions that were used for the pilot scale plant were applied to four different simulations, as described above (Table 1).

2.2. Analysis and selection of modeling particles

The particle size distribution for the influent and effluent water samples in the sedimentation tanks mounting the adjustable baffle was analyzed using a laser diffraction particle size analyzer (LS230, Beckman Coulter) that employed the polarization intensity differential scattering method. A total of 10 samples were collected from both the influent and effluent water at 3-h intervals. Particle size measurements in well-mixed conditions took place immediately after sampling to avoid the aggregation of spherical particles over time.

Fig. 2 depicts the volume fraction of observed particles for the influent (thick line) and effluent water samples (thin line) at the temperature of 27 ± 1 °C. In the figure, the size of particles in the effluent was found to be much smaller than in the influent, indicating that most large particles (> 120 μm) were completely removed from the sedimentation process. An average particle size of 90 μm in the influent was subsequently used for all simulation studies (Table 1). The simulation results using this specific particle size showed the highest agreement with the observed data in terms of the residence time distribution of the conservative tracer and reference particle (Fig. 3), as compared to other frequently

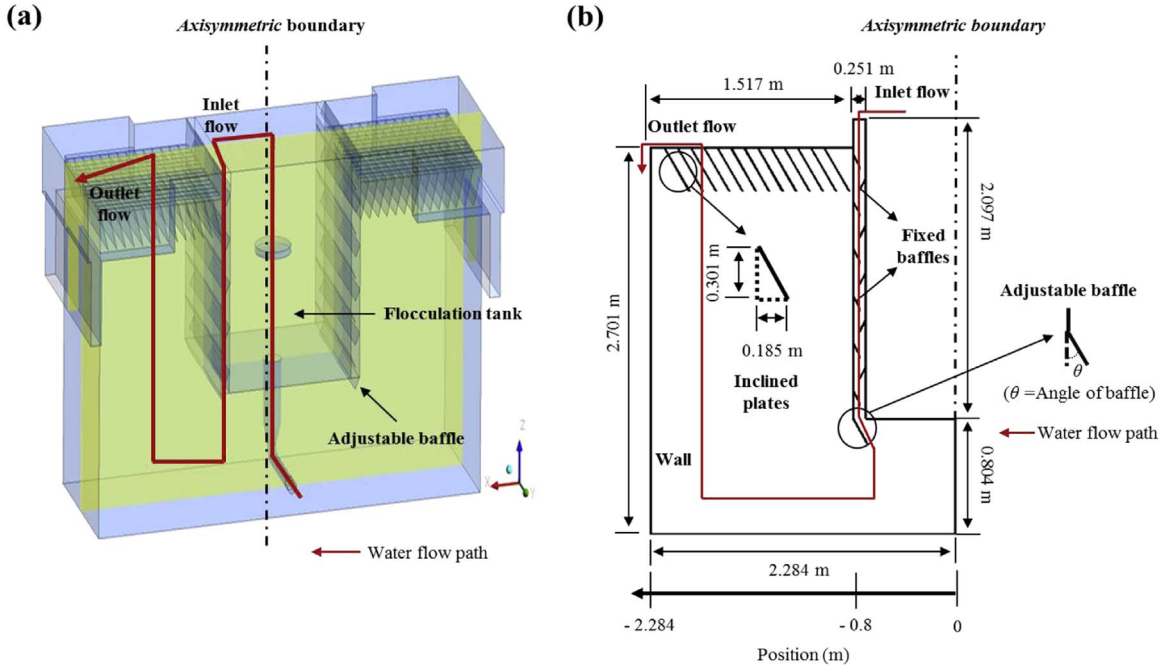

Fig. 1. Schematic diagram of sedimentation tank equipped with fixed and adjustable baffles: (a) a full framework view of model domain in 3 dimensions and (b) geometric view of the left-hand symmetry in 2 dimensions. The thick arrow shown as red color in (a) and (b) indicates the water flow path from the flocculation tank to the sedimentation tank. The influent to the sedimentation tank passes through fixed and adjustable baffles, which maintain the flow and particle patterns constantly and variably, respectively. Position (m) in (b) signifies the distance from the center of the tank to the wall (see Fig. 5). (For interpretation of the references to color in this figure legend, the reader is referred to the web version of this article.)

Table 1
Operating (or simulation) conditions for sedimentation tank with and without adjustable baffles.

Parameters	Values	Units
Average inflow rate	0.0657	m/s
Volumetric loading rate	5.78e−3	m^3/s
Diameter at an inlet channel	0.094	m
Turbulence intensity	5	%
Turbulence length scale	Inlet channel diameter*0.07	m
Water viscosity	1×10^{-3}	Pa s
Water density	1000	kg/m^3
Particle density in a soil-fluid mixture	1054	kg/m^3
Volume fraction of a solid phase at an inlet	0.217	%
Particle diameter	90	μm
Simulation time step	10	s
Particle relaxation time step	1	s

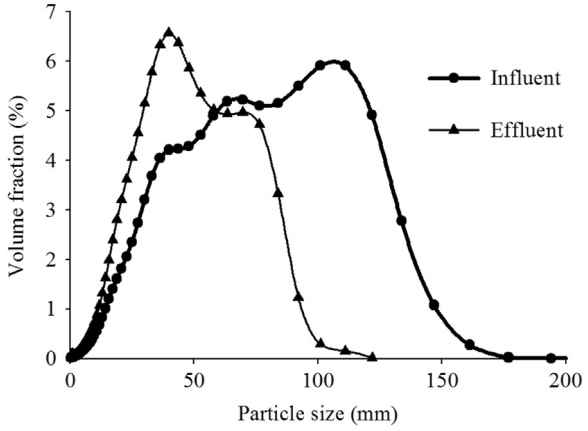

Fig. 2. Particle size distribution of the influent and effluent in sedimentation tank equipped with fixed and adjustable baffles. Each line indicates the average of the entire samples ($n=10$).

detected particles ranging between 50 μm and 100 μm...

2.3. Governing equations

The Euler-Euler approach simultaneously describes the fluid flow and particle motion from a mixture model of turbulent flow and particle tracing, thus allowing us to assess their transient behaviors in the sedimentation tank. In this study, we assumed a fluid-particle mixture as a Newtonian incompressible turbulent fluid, while previous studies often described it as a non-Newtonian fluid due to its viscous flow patterns such as secondary sludge. However, it has been generally observed that as the fluid contained more fine particles, it followed the patterns of a Newtonian fluid closely (Rodríguez López et al., 2008). The transport, continuity, and momentum equations for a solid-fluid mixture can be written, respectively, as:

$$\frac{\partial}{\partial t}(\phi_d\rho_d) + \nabla\cdot(\phi_d\rho_d u_d) = -\, m_{dc} \tag{1}$$

$$(\rho_c - \rho_d)\left[\nabla\cdot(\phi_d(1-c_d)u_{slip} - D_{md}\nabla\cdot(\phi_d) + \frac{m_{dc}}{\rho_d}\right] + \rho_c(\nabla\cdot u) = 0 \tag{2}$$

$$\rho u + \rho(u\cdot\nabla)u = -\nabla p - \nabla\cdot\left[\rho_d c_d(1-c_d)(u_{slip} - \frac{D_{md}}{(1-c_d)\phi_d}\nabla\phi_d)(u_{slip} - \frac{D_{md}}{(1-c_d)\phi_d}\nabla\phi_d)\right] - \nabla\cdot\tau_{Gm} + \rho g + F \tag{3}$$

where ϕ_d refers to the volume fraction of the dispersed phase (i.e., the particle). The density of the mixture fluid, the dispersed phase, and the continuous phase (i.e., the fluid) are indicated by ρ, ρ_d, and ρ_c, respectively. m_d is the mass of the dispersed phase and m_{dc} represents the mass transfer rate between the dispersed and continuous phases. u denotes the velocity of mixture fluid, whereas u_d and u_{slip} indicate the dispersed phase velocity and relative velocity between the two phases, respectively. τ_{Gm} is the sum of viscous and turbulent stress and g is the gravity vector. D_{md} is a turbulent dispersion coefficient and F represents any additional volume force. In this model, it is assumed that both of continue phase and dispersed phase share the same pressure field and the density for each phase is constant in fluid field and each cell.

For turbulence modeling, we used the Reynolds Averaged Navier (RANS) equations (namely, k-ε turbulent model). It solves two additional variables for the transport equations-turbulent kinetic energy $k$and dissipation rate of kinetic energy, ε, which are calculated by following equations,

$$\rho\frac{\partial k}{\partial t} + \rho u\cdot\nabla k = \nabla\cdot\left(\left(\mu + \frac{\mu_T}{\sigma_k}\right)\nabla k\right) + P_k - \rho\varepsilon \tag{4}$$

$$\rho\frac{\partial \varepsilon}{\partial t} + \rho u\cdot\nabla\varepsilon = \nabla\cdot\left(\left(\mu + \frac{\mu_T}{\sigma_\varepsilon}\right)\nabla\varepsilon\right) + C_{\varepsilon1}\frac{\varepsilon}{k}P_k - C_{\varepsilon2}\rho\frac{\varepsilon^2}{k} \tag{5}$$

where σ_k, σ_ε, $C_{\varepsilon1}$, and $C_{\varepsilon2}$ are the model parameters obtained

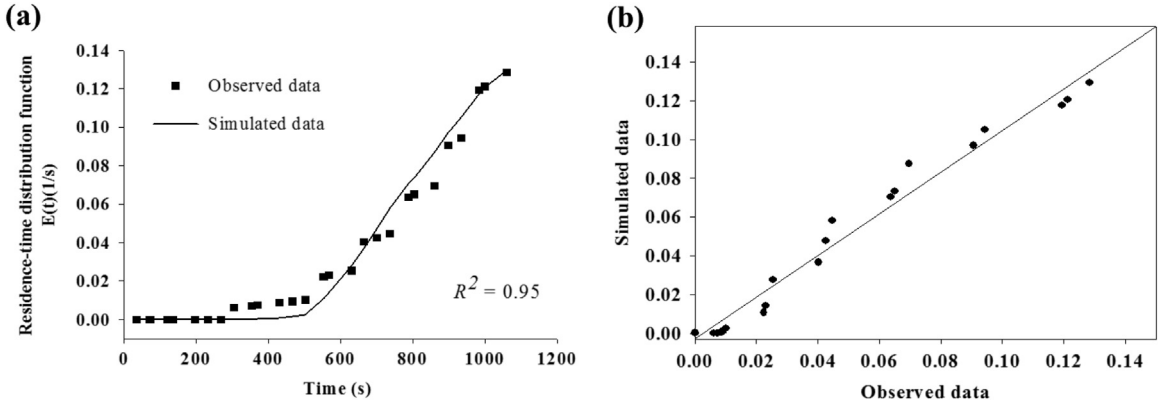

Fig. 3. Comparison of the observed (for a chloride tracer) and simulated residence time distributions of the effluent (for a non-reactive spherical particle of 90 μm) in sedimentation tank with the adjustable baffle inclined at 30° during the initial experimental period (1200 s).

through an optimized data fitting for different levels of turbulent flows. $\mu$is the viscosity of the mixture fluid, and P_k refers to the production term (for the Reynolds stress) which is calculated as follows.

$$P_k = \mu_T\left(\nabla u: \left(\nabla u + (\nabla u)^T\right) - \frac{2}{3}(\nabla\cdot u)^2\right) - \frac{2}{3}\rho k\nabla\cdot u \tag{6}$$

To simulate the slip velocity (u_{slip}) between the dispersed and continuous phases, we selected the Schiller-Neumann formula for the equation of the slip velocity.

$$\frac{3}{4}\frac{C_d}{d_d}\rho_c|u_{slip}|u_{slip} = -\frac{(\rho-\rho_d)}{\rho}\left(-u_t - (u\cdot\nabla)u + g + \frac{F}{\rho}\right) \tag{7}$$

where F means the volume force (N/m^3). The drag coefficient for this formula is defined as:

$$C_d = \frac{24}{\mathrm{Re}_p}\left(1 + 0.15\mathrm{Re}_p^{0.687}\right),\ \mathrm{Re}_p < 1000 \tag{8}$$

$$C_d = 0.44,\ \mathrm{Re}_p > 1000 \tag{9}$$

where C_d indicates the particle drag coefficient and Re_p is the particle Reynolds number. The modified Krieger-Dougherty model enables an estimation of the dynamic mixture viscosity (Struble and Sun, 1993). The viscosity of a medium (or the fluid) will increase with the addition of particles, which is expressed as:

$$\mu = \mu_c\left(1 - \frac{\phi_d}{\phi_{\max}}\right)^{-[\mu]\phi_{\max}} \tag{10}$$

where μ is the total viscosity and μ_c indicates the viscosity of the continuous phase. Φ_{max} represents the maximum packing concentration. The intrinsic viscosity [μ] is set to 2.5 for spherical particles.

The Euler-Euler approach did not calculate the particle trajectory individually, unlike the Euler-Lagrange approach. Accordingly, a particle tracing model based on the Newton's second law was employed to simulate the transient behaviors of each particle. The momentum equation for particles is given as:

$$\frac{d}{dt}(m_p v) = F_D + F_g + F_{ext} \tag{11}$$

$$F_D = \left(\frac{1}{\tau_p}\right)m_p(u_f - u_p) \tag{12}$$

where F_D, F_g, and F_{ext} are the drag, gravity, and external forces, respectively. m_p is the mass of particles and τ_p represents the particle velocity response time. u_f and u_p refer to the velocities of the fluid and particle, respectively. The particle relaxation time for each particle is then estimated from:

$$\tau_p = \frac{\rho_p d_p^2}{18\mu} \tag{13}$$

where ρ_p and d indicate the density and diameter of the particle, respectively. We set the particle relaxation time as 1 s, which was much shorter than the simulation time interval 10 s. Note that an additional term for the turbulent fluctuation u' is added to the mean velocity U to calculate the drag force used in the turbulent flow motion, such that:

$$u_f = U + u' \tag{14}$$

where

$$u' = \zeta\sqrt{\frac{2k}{3}} \tag{15}$$

ζ is the random number normally distributed with zero mean and unit standard deviation. k represents the turbulent kinetic energy.

In reality, the boundary layer effect is typically observed at the interior walls in the sedimentation tank. Adams and Rodi assumed the walls as a smooth surface as the low velocity was prevailed in a large viscous layer (Adams and Rodi, 1990). However, the hydraulic behaviors near the wall surface in the sedimentation tank with complex geometry or compact size were expected to experience high gradient changes due to flow and particle collisions. For this reason, we used the standard wall function developed by Launder and Spalding (1974). The standard wall function imposes the no slip boundary condition for the solid wall in the turbulent flow motion and therefore can be applied to the thin region with large gradient flows.

2.4. Numerical simulation

COMSOL Multiphysics software (version. 4.0) was used to describe the dynamic behavior of the fluid and particle in the sedimentation tank. The FEM was applied to solve the partial differential equations in the 2-dimensional geometry of the sedimentation tank (Fig. 1b). Note that the FEM provides a higher order of accuracy with better geometric flexibility than the FVM. It also has a high stability for a discontinuous solution of the solid-fluid field, but requires high computational resources (Jeon and Shin, 2009; Ren and Leung, 2013). Before starting each simulation, meshes of different sizes were constructed in the geometric domain of the sedimentation tank. Specifically, a fine triangular-type mesh was generated on the fixed and adjustable baffles, inclined plates, and each corner of the sedimentation tank because these regions were expected to show high fluid and particle fluctuations. Conversely, the remaining parts, i.e., all surfaces in the model domain that created 8 individual boundary layers, had a coarse mesh. The different sets of mesh nodes (ranging from 30,000 to 100,000) were tested with respect to the simulation accuracy, numerical stability, convergence, and computational time. From these tests, 100,000 mesh elements and 2800 boundary elements were finally determined and used for the subsequent modeling study. The overall runtime of individual simulations varied between 380 min (for the adjustable baffle inclined at 30°) and 420 min (without the adjustable baffle) using a quad-core processor (i.e., Intel Core i7-4770 3.4 GHz CPU) with 32 GB of memory (Table 1).

The fluid and particle phases in the solid-fluid filed can be solved simultaneously using the Euler-Euler approach (see Section 3). The governing equations for continuity and momentum equations were transformed into a similar homogeneous type, considering both the fluid and particle phases under the assumption that the particle phase always traveled with its terminal velocity relative to the fluid phase. The slip velocity between these two phases was calculated from the drag and body force results from the difference of density between the fluid and particle phases assuming a local equilibrium. This approach is an alternative to the simulation of diluted solid particles in liquids (Manninen et al., 1996). Once the fluid motion of the mixture model was computed, 9000 particles were tracked using the particle tracing model, which accounted for the dynamic behaviors of particles sufficiently in the sedimentation tank. Converged solutions were obtained when changes in the variables of interest at two different time steps were less than 10^{-6}.

Finally, the Morrill index (MI), calculated as T_{90}/T_{10}, was used to investigate the mixing characteristics (or the level of dispersion) in

the sedimentation tank. T_{10} and T_{90} indicate the times when 10% and 90% of particles initially presented in the sedimentation tank disappear, respectively. The small MI value refers to a low level of mixing at a high level uniformity of the hydraulic behaviors (thereby indicating a high particle settling efficiency in the sedimentation tank), and vice versa (Gualtieri and Doria, 2007).

3. Results and discussion

3.1. Model validation

Model validation is a critical step in assessing the reliability of a numerical model that is used to understand the dynamic sedimentation tank processes. Fig. 3 shows the observed and simulated residence time distributions (i.e., the chloride tracer vs 90 μm particle) in the sedimentation tank effluent during an initial 1200 s experimental period. The predicted concentration of the particles was obtained from a reference model output for a sedimentation tank mounting the adjustable baffle inclined at 30° under specific operating conditions (Table 1). We assumed that the chloride tracer and non-reactive spherical particles exhibited a similar transport behavior in the sedimentation tank. In the figure, the (simulated) response time of a 90 μm particle was in excellent agreement with the (observed) response time of the tracer (R^2=0.98 and NSE=0.97). This indicates that our numerical model successfully simulates the transient behavior of the sedimentation tank, and thus can be used to analyze the flow patterns and particle motion in detail.

3.2. Analysis of flow patterns in sedimentation tank

The sedimentation tank mounting the adjusted baffle may greatly affect the flow field and mixing regime, which are directly related to the particle removal efficiency. Zhou and McCorquodale (1992) studied the role of the interior baffle in the flow motion, and found that the kinetic energy of incoming flow and short-circuiting changed significantly depending on its location. Fig. 4a, b, c, and d illustrate how the flow fields in the sedimentation tank are influenced by the absence and presence of the adjustable baffle at 30°, 45°, and 60°. The color bar depicts the fluid velocity and the solid lines represent the streamlines indicating the direction of flow within the boundary of the sedimentation tank (with distances of 0.05 m between streamline positions). The simulation results showed that the influent water flowed from the inlet to the bottom of the sedimentation tank, forming recirculation eddies in two dominant regions (i.e., X and Y) after diverging from the bottom. However, various intensities of recirculation eddies were observed among the adjustable baffle at different angles (compare Fig. 4b, c, and d), in addition to between that without and with the adjustable baffle (compare Fig. 4a and any of Fig. 4b, c, and d). The recirculation eddies generated by the adjustable baffle were found to be larger than those without the adjustable baffle near the area X..

Fig. 5a, b, c, and d present variations of the turbulence kinetic energy, turbulence dissipation rate, (fluid) flow velocity, and horizontal (fluid) flow velocity according to the position of the sedimentation tank. Note that the (fluid) flow velocity is estimated from the model at the location directly below the inclined plates, unlike the other parameters which are at the bottom of the sedimentation tank. From Fig. 5a and b, it was found that the

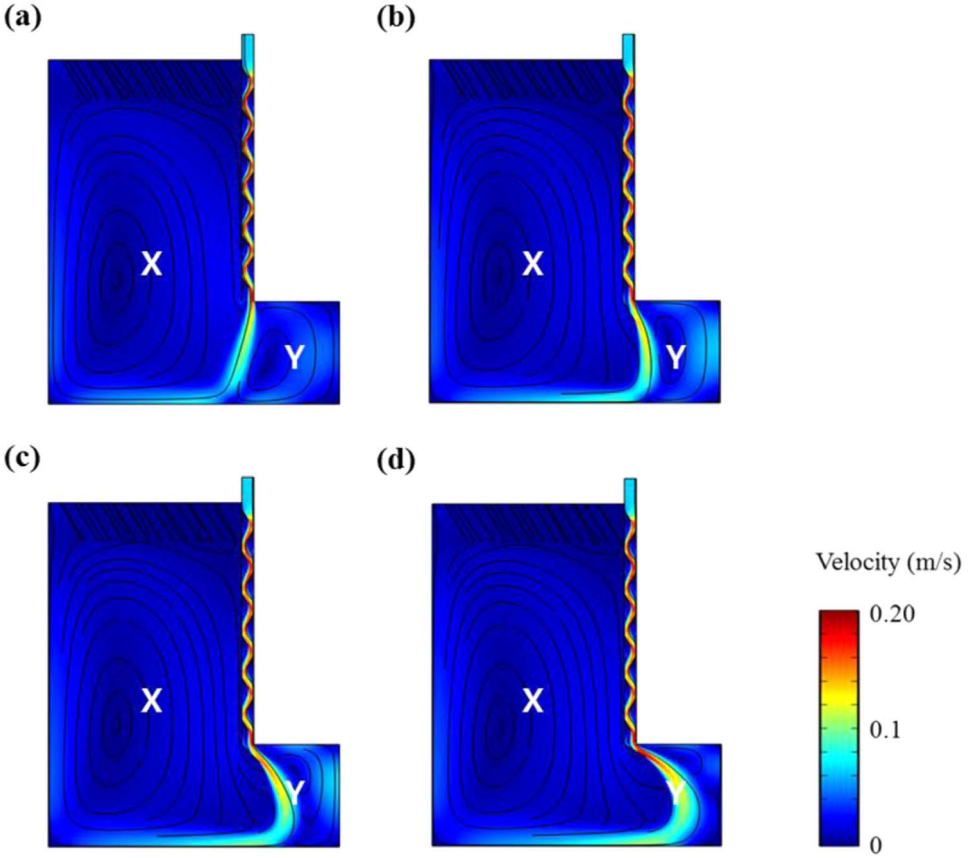

Fig. 4. Velocity contour maps simulated in sedimentation tank (a) without and with adjustable baffle at (b) 30°, (c) 45°, and (d) 60° angles. In the figures, individual solid lines indicate the fluid streamlines and the color bar signifies the velocity. *X* and *Y* denote different areas of interest in a 2 dimensional model domain.

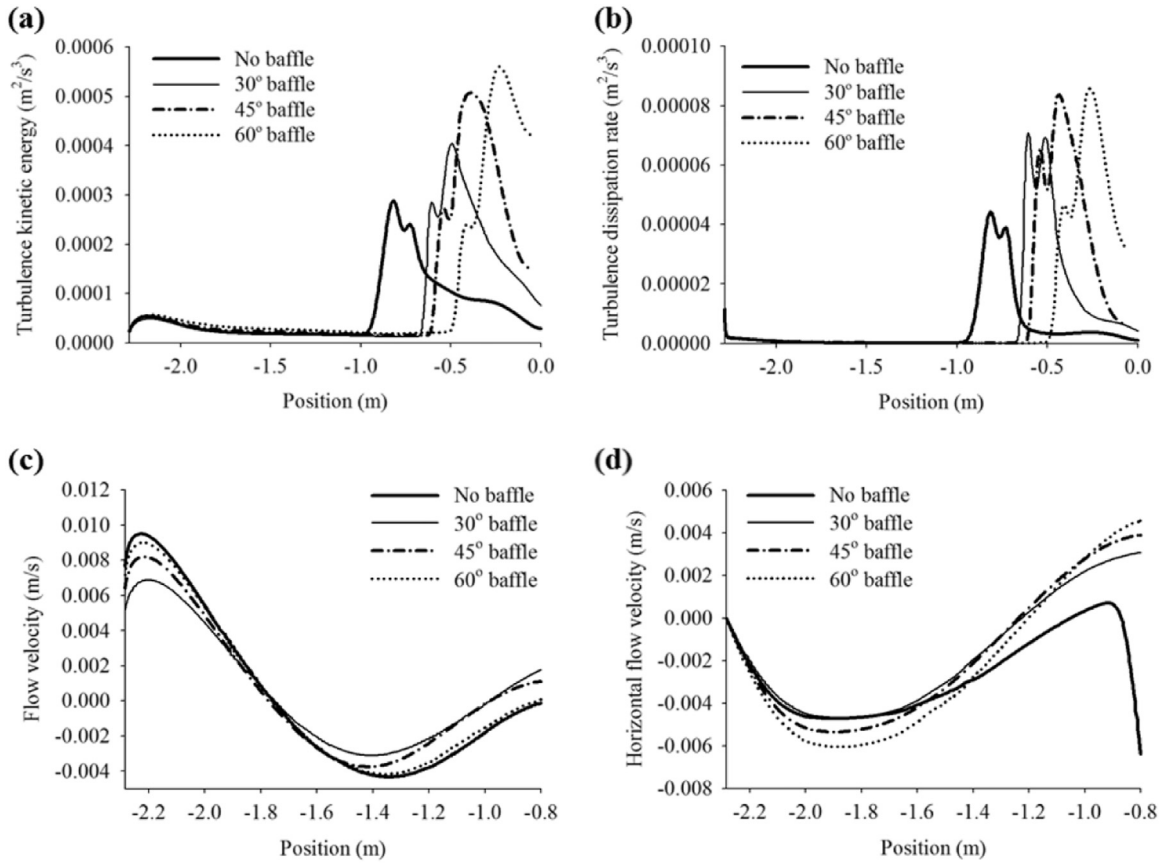

Fig. 5. Simulation results in sedimentation tank without and with adjustable baffle at 30°, 45°, and 60° angles: (a) turbulence kinetic energy (m^2/s^3), (b) turbulence dissipation rate (m^2/s^3), (c) overflow rate (m/s), and (d) horizontal flow rate (m/s). Note that the overflow rate is computed directly below the inclined plates, whereas the remaining parameters are estimated at the bottom of the sedimentation tank (see Fig. 1a). The negative values in position indicate the distance away from the axisymmetric boundary, the center of the entire tertiary sedimentation tank system (see Fig. 1b).

sedimentation tank mounting adjustable baffle considerably increased the turbulence kinetic energy and turbulence dissipation rate in the area of Y. Specifically, as the kinetic energy dissipation rate increased, the recirculation eddies in the area of Y became smaller due to the high momentum loss in the sedimentation tank (Fig. 4a, b, c, and d, and Fig. 5b)..

The low overflow motion around the outlet can be expected as the degree angle of the adjustable baffle that controls the direction of flow inside the sedimentation tank increases from 30° to 60°. However, a higher fluid flow velocity "near the wall", was observed for the adjustable baffle at 60° than for the other angles of the adjustable baffle, although this pattern was reversed in the downward fluid flow (Fig. 5c). When we investigated the velocity profiles inside the sedimentation tank, the adjustable baffle at 60° generated the highest horizontal fluid flow velocity near the wall (lowest velocity in Fig. 5d). Note that in the figure, the negative and positive velocities indicate the direction of horizontal fluid flow to the left and right sides of the wall, respectively. This speedy fluid flow, in turn, caused the highest overflow motion around the outlet among the three different angles in the adjustable baffle.

Remarkably, the adjustable baffle at 30° exhibited lower flow velocity in terms of horizontal and vertical directions than that of 60° (Fig. 5c and d). The sedimentation tank with no baffle exhibited a high overflow motion around the outlet (Fig. 5c), but its horizontal fluid flow velocity was the lowest near the left side of the wall (Fig. 5d) as its fluid flow rebounded directly from the bottom, which minimized the flow velocity in transverse direction. In this situation, fewer particles were likely to be deposited at the bottom, thereby reducing the particle removal efficiency of the sedimentation tank (Adamsson et al., 2003). Therefore, the inclined angles of the adjustable baffle play an important role in enhancing the fine particle sedimentation in the sedimentation tank.

3.3. Analysis of particle motion in sedimentation tank

The particle removal efficiency is known to be affected by the physical characteristics of the solid particles as well as the flow field and mixing regime. Theoretically, as the size of particles decreases, the settling efficiency correspondingly decreases due to inherent properties such as mass and inertia. The particle size distribution of the influent water to the sedimentation tank in our study (Fig. 2) was much smaller than the influent water of the secondary sedimentation tank in another study (Al-Sammarraee et al., 2009). Table 2 presents the particle removal efficiencies observed from the sedimentation tank for the adjustable baffle at

Table 2
Observed particle removal efficiencies for individual particle classes in sedimentation tank having adjustable baffle at a 30° angle.

Particle class	Mean particle diameter (μm)	Volume fraction (%)	Removal efficiency (%)
1	20	0.043	45
2	40	0.386	56
3	60	0.330	64
4	80	0.192	86
5	100	0.039	90
6	120	0.009	99
Average			73

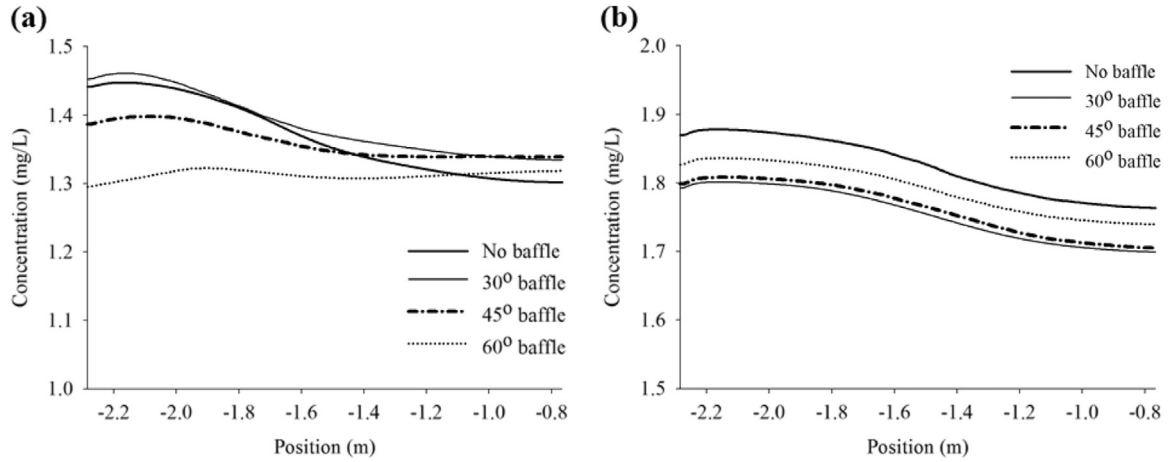

Fig. 6. Predicted concentrations of particles in the effluent (directly below inclined plates) of sedimentation tank with the adjustable baffle inclined at 30°, 45°, and 60° and without one: after (a) 30 and (b) 60 min.

30°. In the table, the particle size removal efficiency varied with each individual particle classes, with an average efficiency of 73%. As expected, this efficiency was lower than previously reported, in which an 87% average removal efficiency was achieved for particles in a secondary sedimentation tank ranging between 20 μm and 850 μm in size (Al-Sammarraee et al., 2009). However, when we compared particles that were less than 120 μm only, the observed removal efficiency of fine particle was always higher than the study that employed a rectangular settling tank having dimensions of 20 m length, 3 m width, and 1.0–2.5 m height (Al-Sammarraee et al., 2009). This finding reflects the fact that the flow control device such as the adjustable baffle in the sedimentation tank has a significant effect on the particle removal efficiency, in addition to the size of particles.

Next, we investigated how the geometry of the system affected the particle motion in more detail using numerical simulation results. Fig. 6 presents the predicted concentrations of particles in the effluent water at the sediment tank under four different flow patterns (i.e., no baffle, 30°, 45°, and 60° baffles) at 30 and 60 min. In the figure, the position (having a negative value) indicates the location away from the adjustable or fixed baffles in the horizontal direction. The predicted concentrations of particles seemed to vary considerably among the different flow patterns during the initial 30 min (Fig. 6a), but showed a more stabilized pattern for the next 30 min (Fig. 6a). After 60 min, the concentrations of particles in the effluent water using adjustable baffle were always lower than with no baffle. The main reason was that more particles were trapped as the recirculation eddies formed circular paths in narrower system boundaries. In fact, a low settling efficiency for small particles (< 120 μm) was observed in the wide system boundary. Overall, the predicted concentrations of particles were the lowest for the 30° baffle, indicating the best particle removal efficiency among the three different angles of the adjustable baffle..

3.4. Analysis of hydraulic behavior for adjustable baffle

To understand whether the mixing characteristics influence the particle sedimentation tank under the influence of the adjustable baffle, the hydraulic behavior in the sedimentation tank was further studied using the MI. Clark (2012) suggested that efficient sedimentation was derived from an ideal plug flow. A low settling performance of particles was observed under the perfect-mix conditions. Based on this understanding, the sedimentation tank should be mixed as little as possible in order to achieve the most efficient fine particle sedimentation, which is indicated by a low MI value. Fig. 7 illustrates the variations of MI values in the

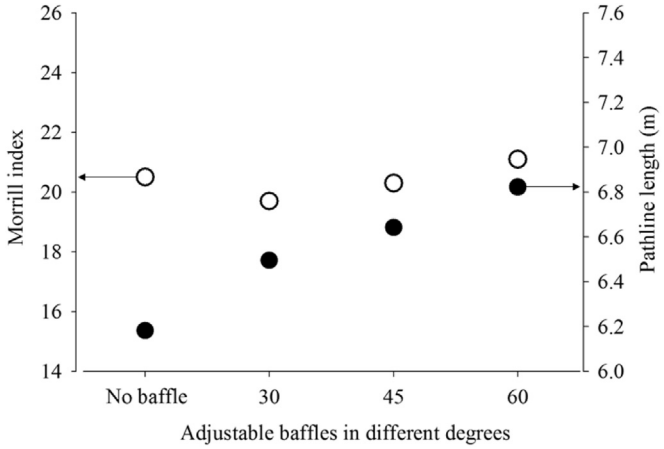

Fig. 7. Changes in the Morrill index and length of particle pathlines for sedimentation tank with the adjustable baffle inclined at 30°, 45°, and 60°, as compared to that without such baffle.

absence and presence of the adjustable baffle at different angles (i.e., 30°, 45°, and 60° see left axis). From the figure, the adjustable baffle at 30° had the lowest MI value; as it approached the ideal plug flow condition, the 30° baffle was seen to provide the best particle removal efficiency. Interestingly, the 60° baffle presented a higher MI value than no baffle condition, which was in contrast to the results of the particle motion (Fig. 6b). This intriguing finding subsequently makes us to explore another index, the length of particle pathlines, which reflects the mixing characteristics in the sedimentation tank in another way..

In Fig. 7, the length of particle pathlines is depicted based on the four flow patterns (see right axis). In the figure, though the sedimentation tank with no adjustable baffle recorded the shortest length of the pathline, the length of pathline kept increasing with the increase of angles in the adjustable baffle, suggesting that there was a greater opportunity for particles to be deposited in the 60° baffle than for the no baffle. However, the length of pathline could not be solely used to indicate the particle settling efficiency, as the value for the 30° baffle was still lower than for the 60° baffle. Note that in the analysis of the particle motion, the best removal efficiency was observed for the 30° baffle (Fig. 6b). Therefore, both indices—the MI and pathline length—play complementary roles in elucidating the mixing characteristics in the system, and should be further evaluated through numerical simulations for a given geometry.

4. Conclusion

In this study, we evaluated the effect of (angles of) the adjustable baffle on the fine particle removal efficiency in the compact sedimentation tank in terms of the flow patterns, particle motion, and mixing characteristics. The mixture model of the solid-fluid field, which was solved concurrently by the Euler-Euler approach in the COMSOL software, was used to describe how the adjustable baffle in the sedimentation tank affect the fine particle sedimentation. A series of numerical simulations based on the experimental data from the pilot scale tank were conducted by modifying the sedimentation tank configurations (i.e., no baffle as well as adjustable baffle at 30°, 45°, and 60°). The main conclusions drawn from this study are as follows.

- The numerical simulation results agreed very well with the observations from the pilot study, the sedimentation tank having the adjustable baffle at 30° (NSE = 0.97).
- The sedimentation tank generated two dominant recirculation eddies in different regions, at a large area (where a flow rebounds from the bottom) when mounted with the adjustable baffle of various angles and at a small area (where the flow curves to the sidewall) without the adjustable baffle. Overall, the overflow rate changed significantly due to the angles of the adjustable baffle, which revealed that they were a decisive factor of controlling the removal of fine particles in the sedimentation tank.
- The average particle removal efficiency was estimated to be 73%, which was lower than a previous study that evaluated a rectangular tank with a long length (87%). However, the removal efficiency was higher than the previous study when considering fine particles ($< 120\ \mu m$) only, indicating that the geometry of the sedimentation tank considerably affected the particle removal efficiency. This mechanism was clearly seen over time, especially after the motion of particles in the sedimentation tank became stabilized.
- The MI values, which illustrate the mixing characteristics in a given system, in descending order are: the 60° baffle, no baffle, the 45° baffle, and the 30° baffle. The most efficient sedimentation (indicated by the low MI value) was achieved by the 30° baffle. However, the MI values alone did not always correctly describe the fine particle sedimentation in the system. The reason was that the 60° baffle was found to deposit more particles than the sedimentation tank without the adjustable baffle when considering particle motion and pathline length.
- Therefore, we recommend that numerical simulations should be conducted in the design of the sedimentation tanks, as this will not only help to explain the hydraulic behaviors of the system, but considerably improve the fine particle removal efficiency. To a large extent, this research provides new insights into the novel design of the compact sedimentation tanks for advanced water treatment to improve the process efficiency.

Acknowledgments

This work is supported by the Korea Agency for Infrastructure Technology Advancement(KAIA) grant funded by the Ministry of Land, Infrastructure and Transport (Grant 1615007273).

References

Adamczyk, W.P., Klimanek, A., Białecki, R.A., Węcel, G., Kozołub, P., Czakiert, T., 2014. Comparison of the standard euler–euler and hybrid Euler–Lagrange approaches for modeling particle transport in a pilot-scale circulating fluidized bed. Particuology 15, 129–137.

Adams, E.W., Rodi, W., 1990. Modeling flow and mixing in sedimentation tanks. J. Hydraul. Eng. – ASCE 116, 895–913.

Adamsson, Å., Stovin, V., Bergdahl, L., 2003. Bed shear stress boundary condition for storage tank sedimentation. J. Environ. Eng. – ASCE 129, 651–658.

Al-Sammarraee, M., Chan, A., Salim, S.M., Mahabaleswar, U.S., 2009. Large-eddy simulations of particle sedimentation in a longitudinal sedimentation basin of a water treatment plant. Part I: particle settling performance. Chem. Eng. J. 152, 307–314.

Brouckaert, C.J., Buckley, C.A., 1999. The use of computational fluid dynamics for improving the design and operation of water and wastewater treatment plants. Water Sci. Technol. 40, 81–89.

Clark, M.M., 2012. Transport Modeling For Environmental Engineers and Scientists, 2nd ed. John Wiley & Sons, New Jersey.

DeVantier, B.A., Larock, B.E., 1986. Modelling a recirculating density-driven turbulent flow. Int. J. Numer. Methods Fluids 6, 241–253.

DeVantier, B.A., Larock, B.E., 1987. Modeling sediment-induced density currents in sedimentation basins. J. Hydraul. Eng. – ASCE 113, 80–94.

Gohil, T., McGregor, R.H.P., Szczerba, D., Burckhardt, K., Muralidhar, K., Székely, G., 2011. Simulation of oscillatory flow in an aortic bifurcation using FVM and FEM: a comparative study of implementation strategies. Int. J. Numer. Methods Fluids 66, 1037–1067.

Goula, A.M., Kostoglou, M., Karapantsios, T.D., Zouboulis, A.I., 2008a. A CFD methodology for the design of sedimentation tanks in potable water treatment: case study: the influence of a feed flow control baffle. Chem. Eng. J. 140, 110–121.

Goula, A.M., Kostoglou, M., Karapantsios, T.D., Zouboulis, A.I., 2008b. The effect of influent temperature variations in a sedimentation tank for potable water treatment—a computational fluid dynamics study. Water Res. 42, 3405–3414.

Gualtieri, C., Doria, G.P., 2007. Residence time distribution and dispersion in a contact tank, in: Proceedings of the XXXII IAHR Congress, Venice, Italy, p. 486.

Jeon, W., Shin, C.B., 2009. Design and simulation of passive mixing in microfluidic systems with geometric variations. Chem. Eng. J. 152, 575–582.

Karama, A.B., Onyejekwe, O.O., Brouckaert, C.J., Buckley, C.A., 1999. The use of computational fluid dynamics (CFD). Technique for evaluating the efficiency of an activated sludge reactor. Water Sci. Technol. 39, 329–332.

Larsen P., 1977. On the Hydraulics of Rectangular Settling Basins: Experimental and Theoretical Studies. Report No. 1001. Department of Water Resources Engineering, Lund Institute of Technology, Lund University, Lund, Sweden.

Launder, B.E., Spalding, D., 1974. The numerical computation of turbulent flows. Comput. Methods Appl. Mech. Eng. 3, 269–289.

Loha, C., Chattopadhyay, H., Chatterjee, P.K., 2014. Effect of coefficient of restitution in Euler–Euler CFD simulation of fluidized-bed hydrodynamics. Particuology 15, 170–177.

Lyn, D., Stamou, A., Rodi, W., 1992. Density currents and shear-induced flocculation in sedimentation tanks. J. Hydraul. Eng. – ASCE 118, 849–867.

Manninen, M., Taivassalo, V., Kallio, S., 1996. On the mixture model for multiphase flow. VTT Publications 288, Technical Research Centre of Finland, pp. 1–67.

McCorquodale, J., Yuen, E., Vitasovic, Z., Samstag, R., 1991. Numerical simulation of unsteady conditions in clarifiers. Water Poll. Res. J. Can. 26, 201–222.

Patziger, M., Kainz, H., Hunze, M., Józsa, J., 2012. Influence of secondary settling tank performance on suspended solids mass balance in activated sludge systems. Water Res. 46, 2415–2424.

Ren, Y., Leung, W.W.-F., 2013. Flow and mixing in rotating zigzag microchannel. Chem. Eng. J. 215–216, 561–578.

Rodríguez López, P., Lavín, A.G., Mahamud López, M.M., Bueno de las Heras, J.L., 2008. Flow models for rectangular sedimentation tanks. Chem. Eng. Process. 47, 1705–1716.

Struble, L.J., Sun, G.-K., 1993. Cement viscosity as a function of concentration, in: Proceedings of the Materials Research Society Symposium. Cambridge University Press, pp. 173–173.

Szalai, L., Krebs, P., Rodi, W., 1994. Simulation of flow in circular clarifiers with and without swirl. J. Hydraul. Eng. – ASCE 120, 4–21.

Tarpagkou, R., Pantokratoras, A., 2013. CFD methodology for sedimentation tanks: The effect of secondary phase on fluid phase using DPM coupled calculations. Applied Mathematical Modelling 37, 3478–3494.

Tarpagkou, R., Pantokratoras, A., 2014. The influence of lamellar settler in sedimentation tanks for potable water treatment—a computational fluid dynamic study. Powder Technol. 268, 139–149.

Wang, X., Sun, R., Ao, X., Zhou, Z., Lang, J., 2013. Eulerian–eulerian solid–liquid two-phase flow of sandstone wastewater in a hydropower station rectangular sedimentation tank. Eur. J. Environ. Civ. Eng. 17, 700–719.

Zhou, S., McCorquodale, J.A., 1992. Influence of skirt radius on performance of circular clarifier with density stratification. Int. J. Numer. Methods Fluids 14, 919–934.

Zhu, Z., Kamnis, S., Gu, S., 2015. Numerical study of molten and semi-molten ceramic impingement by using coupled eulerian and lagrangian method. Acta Mater. 90, 77–87.